

# Spectroscopic study and astronomical detection of doubly $^{13}\text{C}$ -substituted ethyl cyanide

L. Margulès<sup>1</sup>, A. Belloche<sup>2</sup>, H. S. P. Müller<sup>3</sup>, R. A. Motiyenko<sup>1</sup>, J.-C. Guillemin<sup>4</sup>, R. T. Garrod<sup>5</sup>, and K. M. Menten<sup>2</sup>

<sup>1</sup> Laboratoire de Physique des Lasers, Atomes, et Molécules, UMR CNRS 8523, Université de Lille I, 59655 Villeneuve d'Ascq Cédex, France e-mail: laurent.margules@univ-lille1.fr

<sup>2</sup> Max-Planck-Institut für Radioastronomie, Auf dem Hügel 69, 53121 Bonn, Germany

<sup>3</sup> I. Physikalisches Institut, Universität zu Köln, Zùlpicher Str. 77, 50937 Köln, Germany

<sup>4</sup> Institut des Sciences Chimiques de Rennes, Ecole Nationale Supérieure de Chimie de Rennes, CNRS, UMR 6226, 11 Allée de Beaulieu, CS 50837, 35708 Rennes Cedex 7, France

<sup>5</sup> Departments of Chemistry and Astronomy, University of Virginia, Charlottesville, VA 22904, USA

Received 15 February 2016 / Accepted 9 April 2016

## ABSTRACT

**Context.** We have performed a spectral line survey called EMOCA toward Sagittarius B2(N) between 84.0 and 114.4 GHz with the Atacama Large Millimeter/submillimeter Array (ALMA) in its Cycles 0 and 1. Line intensities of the main isotopic species of ethyl cyanide and its singly  $^{13}\text{C}$ -substituted isotopomers observed toward the hot molecular core Sagittarius B2(N2) suggest that the doubly  $^{13}\text{C}$ -substituted isotopomers should be detectable also.

**Aims.** We want to determine the spectroscopic parameters of all three doubly  $^{13}\text{C}$ -substituted isotopologues of ethyl cyanide to search for them in our ALMA data.

**Methods.** We investigated the laboratory rotational spectra of the three species between 150 GHz and 990 GHz. We searched for emission lines produced by these species in the ALMA spectrum of Sagittarius B2(N2). We modeled their emission as well as the emission of the  $^{12}\text{C}$  and singly  $^{13}\text{C}$ -substituted isotopologues assuming local thermodynamic equilibrium.

**Results.** We identified more than 5000 rotational transitions, pertaining to more than 3500 different transition frequencies, in the laboratory for each of the three isotopomers. The quantum numbers reach  $J \approx 115$  and  $K_a \approx 35$ , resulting in accurate spectroscopic parameters and accurate rest frequency calculations beyond 1000 GHz for strong to moderately weak transitions of either isotopomer. All three species are unambiguously detected in our ALMA data. The  $^{12}\text{C}/^{13}\text{C}$  column density ratio of the isotopomers with one  $^{13}\text{C}$  atom to the ones with two  $^{13}\text{C}$  atoms is about 25.

**Conclusions.** Ethyl cyanide is the second molecule after methyl cyanide for which isotopologues containing two  $^{13}\text{C}$  atoms have been securely detected in the interstellar medium. The model of our ethyl cyanide data suggests that we should be able to detect vibrational satellites of the main species up to at least  $v_{19} = 1$  at  $\sim 1130$  K and up to  $v_{13} + v_{21} = 2$  at  $\sim 600$  K for the isotopologues with one  $^{13}\text{C}$  atom in our present ALMA data. Such satellites may be too weak to be identified unambiguously for isotopologues with two  $^{13}\text{C}$  atoms.

**Key words.** molecular data – methods: laboratory – techniques: spectroscopic – radio lines: ISM – ISM: molecules – ISM: individual objects: Sagittarius B2(N)

## 1. Introduction

Investigations of the warm (100–200 K) and dense parts of high mass star-forming regions known as “hot cores” (or “hot corinos” for their low mass star analogs) have unveiled a wealth of complex molecules. These are saturated or nearly saturated organic molecules for the most part, reaching thus far up to 12 atoms (Belloche et al. 2014). Most of these molecules have been detected toward Sagittarius B2 (Sgr B2 for short). The Sgr B2 molecular cloud complex is one of the most prominent star-forming regions in our Galaxy. It is located close to the Galactic centre and contains two major sites of high-mass star formation, Sgr B2(M) and (N). Sgr B2(N) has a greater variety of complex organic molecules than Sgr B2(M). It contains two dense, compact hot cores which are separated by about  $5''$  in the north-south direction (Belloche et al. 2008; Qin et al. 2011; Belloche et al. 2016). The more prominent one is Sgr B2(N1), also known as the Large Molecule Heimat, and Sgr B2(N2) is to the north of it.

We used the Atacama Large Millimeter/submillimeter Array (ALMA) in its Cycles 0 and 1 to perform a spectral line survey of Sagittarius B2(N) between 84.0 and 114.4 GHz. This survey is called Exploring Molecular Complexity with ALMA (EMOCA). The high angular resolution ( $\sim 1.5$ – $1.8''$ ) achieved in the survey allows us to separate the emission of the two hot cores and reveals that Sgr B2(N2) has relatively narrow linewidths ( $\sim 5 \text{ km s}^{-1}$ ), which reduces the line confusion compared to previous single-dish surveys of Sgr B2(N). Therefore, our analysis has been focused on this source so far. One of the first results of EMOCA has been the first detection in space of a branched alkyl molecule, *iso*-propyl cyanide, which is found to be nearly as abundant as its straight-chain isomer *n*-propyl cyanide (Belloche et al. 2014). The laboratory spectroscopic investigation on *iso*-propyl cyanide (Müller et al. 2011) was an obvious prerequisite. The decrease in line confusion, however, was important also because this molecule was not detected in our previous single-dish survey of Sgr B2(N) (Belloche et al. 2013; Müller et al. 2011).

The lighter ethyl cyanide,  $C_2H_5CN$ , also known as propanitrile, is considerably more prominent than either *iso*- or *n*-propyl cyanide in our ALMA survey. In fact, lines of the three isotopomers with one  $^{13}C$  atom are so strong that we expected to be able to detect those of the three isotopomers with two  $^{13}C$  atoms. The parent isotopic species was detected in the Orion Molecular Cloud and in Sgr B2 (Johnson et al. 1977) soon after the even lighter methyl cyanide was detected (Solomon et al. 1971). The molecule was also detected in the hot corinos of low-mass protostars such as IRAS 16293-2422, NGC 1333-IRAS 2A, and NGC 1333-IRAS 4A (Cazaux et al. 2003; Taquet et al. 2015). Rotational transitions within the two lowest-lying vibrational states were detected in G327.3–0.6 (Gibb et al. 2000) and Sgr B2(N) (Mehring et al. 2004). Transitions of even higher excited states were detected in the high-mass star forming regions Orion KL and Sgr B2(N) (Daly et al. 2013; Belloche et al. 2013). Its  $^{13}C$  isotopomers were detected first in Orion IRC2 (Demyk et al. 2007) and soon thereafter in Sgr B2(N) (Müller et al. 2008). Margulès et al. (2009) reported the detection of  $C_2H_5C^{15}N$  in Orion IRC2.

The rotational spectrum of the parent isotopic species has been studied extensively in its ground vibrational state. The recent work by Brauer et al. (2009) extended the data to 1.6 THz. Information is also available on some low-lying vibrational states (Daly et al. 2013). The ground vibrational states of all singly substituted ethyl cyanide species were studied rather extensively, in particular the ones with  $^{13}C$  (Demyk et al. 2007; Richard et al. 2012), but also the ones with D and  $^{15}N$  (Margulès et al. 2009).

No data are available for  $C_2H_5CN$  isotopomers with two  $^{13}C$  atoms. Therefore, we prepared ethyl cyanide samples highly enriched in  $^{13}C$  at two positions, recorded its rotational spectra up to 1 THz and searched for it in our ALMA data toward Sgr B2(N2). Details about the laboratory experiments and the astronomical observations are given in Sect. 2. Section 3 presents the results of the laboratory spectroscopy and the analysis of the astronomical spectra. These results are discussed in Sect. 4 and the conclusions are given in Sect. 5.

## 2. Experimental details

### 2.1. Synthesis

Into a three-necked flask equipped with a stirring bar, a reflux condenser, and a nitrogen inlet, were introduced triethylene glycol (20 mL), potassium cyanide (0.7 g, 10.7 mmol), and iodoethane- $^{13}C_2$  (1 g, 6.4 mmol). The mixture was heated to 110°C and stirred at this temperature for one hour. After cooling to room temperature, the flask was fitted on a vacuum line equipped with two U-tubes. The high boiling compounds were condensed in the first trap cooled at –30°C and propanenitrile-2,3- $^{13}C_2$  ( $^{13}CH_3^{13}CH_2CN$ ) was selectively condensed in the second trap cooled at –90°C. The reaction was performed starting from stoichiometric amounts of 1-iodoethane- $^{13}C$  and  $K^{13}CN$  to prepare propanenitrile-1,2- $^{13}C_2$  ( $CH_3^{13}CH_2^{13}CN$ ), and starting from 2-iodoethane- $^{13}C$  and  $K^{13}CN$  to prepare propanenitrile-1,3- $^{13}C_2$  ( $^{13}CH_3CH_2^{13}CN$ ). The nuclear magnetic resonance data (NMR) of the three isotopologues is given in Appendix A.

### 2.2. Lille - submillimeter spectra

The measurements in the frequency range under investigation (150–990 GHz) were performed using the Lille spectrometer (Alekseev et al. 2012). A quasi-optic dielectric hollow wave-

guide of 3 m length containing investigated gas at the required pressure was used as the sample cell in the spectrometer. The measurements were done at typical pressures of 10 Pa and at room temperature. The frequency ranges 150–330, 400–660, and 780–990 GHz were covered with various active and passive frequency multipliers from VDI Inc. and an Agilent synthesizer (12.5–18.25 GHz) was used as the source of radiation. Estimated uncertainties for measured line frequencies are 30 kHz and 50 kHz depending on the observed S/N and the frequency range.

### 2.3. Observations

Part of the observations used in this article have been briefly described in Belloche et al. (2014). Here we use the full dataset of the EMoCA survey to search for the emission of the three doubly  $^{13}C$ -substituted isotopologues of ethyl cyanide toward Sgr B2(N2) at the equatorial position  $(\alpha, \delta)_{J2000} = (17^h47^m19.86^s, -28^\circ22'13.4'')$ . In brief, the survey covers the frequency range 84.1 – 114.4 GHz with a spectral resolution of 488.3 kHz (1.7 to 1.3 km s $^{-1}$ ). The angular resolution ranges from 1.4'' to 2.1''. A detailed account of the observations, reduction, and analysis method of the full dataset is reported in Belloche et al. (2016).

## 3. Results

### 3.1. Laboratory spectroscopy

Ethyl cyanide is an asymmetric top rotor with  $\kappa = (2B - A - C)/(A - C) = -0.9591$  for the parent isotopic species, quite close to the prolate limit of –1. The cyano group causes a large dipole moment of 3.816 (3) D along the *a*-inertial axis and a still sizeable 1.235 (1) D along the *b*-inertial axis (Kraśnicki & Kisiel 2011). As a consequence *a*-type transitions dominate the room temperature rotational spectrum up to about 0.75 THz. Internal rotation splitting of the  $CH_3$  group or hyperfine structure splitting caused by the  $^{14}N$  nucleus are only resolvable in selected transitions at low frequencies. Both types of splitting were not resolved here. Heavy atom substitution changes the spectroscopic parameters only slightly, and the changes in the dipole moment components are very small, such that they are usually neglected.

The initial predictions were obtained from scaling data calculated ab initio to values of known isotopic species. The rotational and quartic centrifugal distortion parameters of the doubly  $^{13}C$ -substituted species were calculated with harmonic force field calculations at B3LYP/6-311G++(3df,2pd) level. The same type of calculations were done for the two mono substituted  $^{13}CH_3CH_2CN$  and  $CH_3^{13}CH_2CN$  species, and the differences between the ab initio and experimental values from Richard et al. (2012) were calculated. The scaling values from  $^{13}CH_3CH_2CN$  were added to  $^{13}CH_3CH_2^{13}CN$  and  $^{13}CH_3^{13}CH_2CN$  parameters, and the ones of  $CH_3^{13}CH_2CN$  to  $CH_3^{13}CH_2^{13}CN$ . This method permits to obtain first predictions better than 10 MHz in the lowest part of our frequency range. The *a*R-branch  $J = 18 - 17$  pattern was easily recognised in the spectra around 150 GHz. The assignment procedure was the same for all three species: transitions obeying *a*-type selection rules were assigned up to 330 GHz first, then *b*R- and *b*Q-branch transitions from 150 to 330 GHz. After these first steps all quartic and sextic distortional parameters could be determined. Transitions from 400 to 990 GHz could be assigned subsequently. Transitions with high  $K_a$  values were difficult to assign because

**Table 1.** Spectroscopic parameters of three ethyl cyanide isotopomers with two  $^{13}\text{C}$  atoms in comparison to those of the main isotopologue.

Parameter	$\text{CH}_3\text{CH}_2\text{CN}^a$	$\text{CH}_3^{13}\text{CH}_2^{13}\text{CN}$	$^{13}\text{CH}_3\text{CH}_2^{13}\text{CN}$	$^{13}\text{CH}_3^{13}\text{CH}_2\text{CN}$
<i>A</i>	27663.68206 (52)	27021.85940 (20)	27314.27505 (23)	26713.80045 (26)
<i>B</i>	4714.187784 (80)	4673.123591 (27)	4572.983663 (31)	4584.329843 (36)
<i>C</i>	4235.085063 (74)	4186.641599 (26)	4112.858906 (28)	4107.933715 (34)
$D_K \times 10^3$	547.7770 (29)	530.8139 (12)	551.8269 (18)	523.8704 (14)
$D_{JK} \times 10^3$	-47.26453 (43)	-44.84446 (15)	-48.15240 (17)	-45.53332 (18)
$D_J \times 10^3$	3.008009 (37)	2.8877592 (81)	2.8936301 (90)	2.8561756 (96)
$d_1 \times 10^6$	-685.888 (10)	-674.1535 (29)	-653.1202 (41)	-662.5892 (44)
$d_2 \times 10^6$	-32.7755 (35)	-33.5854 (11)	-29.6589 (20)	-32.1002 (24)
$H_K \times 10^6$	31.3192 (97)	30.1526 (36)	31.6084 (71)	29.9891 (37)
$H_{KJ} \times 10^6$	-1.58325 (89)	-1.52676 (33)	-1.57282 (44)	-1.58070 (36)
$H_{JK} \times 10^9$	-118.60 (14)	-109.219 (44)	-125.624 (53)	-111.647 (50)
$H_J \times 10^9$	9.3563 (74)	8.5651 (10)	8.7869 (12)	8.6217 (11)
$h_1 \times 10^9$	3.9036 (30)	3.67178 (50)	3.64423 (70)	3.63986 (68)
$h_2 \times 10^{12}$	514.09 (97)	508.74 (29)	451.63 (49)	485.59 (44)
$h_3 \times 10^{12}$	63.18 (29)	65.67 (10)	56.59 (18)	61.79 (20)
$L_K \times 10^9$	-2.105 (14)	-1.9089 (36)	-2.0784 (89)	-1.9253 (33)
$L_{KKJ} \times 10^{12}$	83.27 (65)	84.32 (24)	81.30 (34)	88.24 (24)
$L_{JK} \times 10^{12}$	-6.57 (16)	-5.796 (63)	-5.149 (84)	-4.572 (64)
$L_{JJK} \times 10^{12}$	0.522 (19)	0.4905 (49)	0.6057 (63)	0.4825 (55)
$L_J \times 10^{15}$	-42.37 (63)	-31.705 (42)	-33.246 (54)	-32.335 (45)
$l_1 \times 10^{15}$	-21.35 (33)	-17.184 (24)	-17.442 (34)	-17.077 (30)
$l_2 \times 10^{15}$	-4.351 (62)	-4.159 (17)	-3.696 (28)	-3.935 (22)
$l_3 \times 10^{15}$	-1.170 (23)	-1.1694 (85)	-1.011 (14)	-1.074 (14)
$l_4 \times 10^{15}$	-0.1380 (86)	-0.1356 (31)	-0.1138 (32)	-0.1145 (34)
$P_K \times 10^{15}$	113.2 (69)			
$P_{KKJ} \times 10^{15}$				
$P_{KJ} \times 10^{15}$	-1.707 (92)	-1.754 (34)	-1.834 (48)	-1.658 (33)
$P_{JK} \times 10^{15}$	0.1483 (79)	0.0808 (26)	0.0763 (32)	0.0618 (28)
$P_{JJK} \times 10^{18}$	-5.12 (90)	-4.08 (19)	-5.19 (27)	-3.17 (22)
$P_J \times 10^{18}$	0.207 (20)			
$p_1 \times 10^{18}$	0.083 (11)			
$N_{\text{lines}}^b$	—	4586	3686	3580
$\sigma^c$	—	25.9	24.8	28.4
$\sigma_{\text{weighted}}^d$	—	0.860	0.824	0.935

**Notes.** Watson's *S* reduction has been used in the representation *I'*. All parameters are given in MHz except for the last three lines. Numbers in parentheses are one standard deviations in units of the least significant figures. <sup>(a)</sup> Brauer et al. (2009). <sup>(b)</sup> Number of distinct lines. <sup>(c)</sup> Standard deviation of the fit in kHz. <sup>(d)</sup> Weighted deviation of the fit.

these were frequently weaker than transitions pertaining to excited vibrational states and were often blended with these. As is usual for a molecule of this size, many lines remain unassigned because assignments of transitions in excited vibrational states were beyond the scope of the present investigation. Predictions of the spectra were carried out with SPCAT (Pickett 1991), AS-FIT (Kisiel 2001) was employed for fitting. Even though both *A* and *S* reduction of the rotational Hamiltonian perform nearly equally well for ethyl cyanide (Richard et al. 2012), we used the latter (in the *I'* representation) because the molecule is close to the symmetric prolate limit. The final line lists consist of ~6800 transitions for the 1,2-substituted isotopomer and ~5500 for the 1,3- and 2,3-substituted isotopomers. The number of different transition frequencies is smaller, ~4600 and ~3600, respectively, because asymmetry splitting was frequently not resolved, and in some cases accidentally overlapping lines were retained in the fit. The *J* values reach ~115, and  $K_a$  values extend to at least 20 for *b*-type transitions and to around 35 for *a*-type transitions.

We determined for each isotopomer a full set of up to eighth-order rotational parameters along with three diagonal decic parameters. They are presented in Table 1 together with values for the parent isotopologue from Brauer et al. (2009). Predictions of the rotational spectra of the three isotopomers will be available in the catalog section<sup>1</sup> of the CDMS; the line, parameter, and fit files, along with additional auxiliary files, will be provided in the CDMS archive<sup>2</sup>. Supplementary text files S1.txt, S2.txt, S3.txt will be available at CDS. They contain the transitions used in the fit with experimental frequencies, accuracies and residuals from the fits. Table B.1 in the appendix provides guidance on these files.

Rotational partition function values of ethyl cyanide and its three isotopomers containing two  $^{13}\text{C}$  atoms are provided at selected temperatures in Table 2. The temperatures are the standard temperatures in the CDMS (Müller et al. 2001, 2005) and

<sup>1</sup> <http://www.astro.uni-koeln.de/cdms/entries>

<sup>2</sup> <http://www.astro.uni-koeln.de/site/vorhersagen/catalog/archive/EtCN/>

**Table 2.** Rotational partition function values of three ethyl cyanide isotopomers with two  $^{13}\text{C}$  atoms at selected temperatures in comparison to those of the main isotopologue.

$T$ (K)	$Q(\text{CH}_3\text{CH}_2\text{CN})^a$	$Q(\text{CH}_3^{13}\text{CH}_2^{13}\text{CN})$	$Q(^{13}\text{CH}_3\text{CH}_2^{13}\text{CN})$	$Q(^{13}\text{CH}_3^{13}\text{CH}_2\text{CN})$
300.0	37424.5763	38253.0668	38806.4684	39214.7041
225.0	24286.9324	24824.3519	25183.2785	25448.2672
150.0	13209.5867	13501.7478	13696.8350	13840.9909
75.0	4667.9361	4771.1127	4839.9793	4890.9278
37.5	1651.0572	1687.5264	1711.8515	1729.8717
18.75	584.6478	597.5483	606.1417	612.5216
9.375	207.4255	211.9936	215.0286	217.2911

Notes. <sup>(a)</sup> Derived from Brauer et al. (2009).

**Table 3.** Vibrational correction factors to the rotational partition function of ethyl cyanide at selected temperatures.

$T$ (K)	$F_{\text{vib}}$
300.0	3.3438
225.0	2.1318
150.0	1.3848
75.0	1.0384
37.5	1.0007
18.75	1.0000
9.375	1.0000

JPL (Pickett et al. 1998) catalogs. At the elevated temperatures in hot cores, such as Sgr B2(N2), and under the assumption of LTE a considerable part of larger organic molecules is excited to vibrational levels higher than the ground vibrational state. At 150 K a vibrational state at an energy of  $480\text{ cm}^{-1}$  (or 691 K) has a population of 0.01 with respect to  $v = 0$ . The fundamental vibrations of ethyl cyanide have been well determined experimentally (Heise et al. 1981), however, only a selection of overtone and combination levels are known. Therefore, we used the harmonic oscillator approximation, as is commonly done, to evaluate contributions of such states. Use of the anharmonic fundamentals accounts in part for the anharmonicity of the vibrations. The resulting vibrational correction factors to the rotational partition function of the main isotopologue are given in Table 3. Isotopic differences are small and most likely within the errors of the harmonic oscillator approximation for such a heavy molecule as ethyl cyanide.

### 3.2. Detection toward Sgr B2(N2)

The LTE modelling of the ALMA spectrum of Sgr B2(N2) reveals the presence of the three doubly  $^{13}\text{C}$ -substituted isotopologues of ethyl cyanide: about 8, 7, and 8 lines that do not suffer too much from blending with transitions of other species are clearly detected for  $\text{CH}_3^{13}\text{CH}_2^{13}\text{CN}$  (Fig. C.1),  $^{13}\text{CH}_3\text{CH}_2^{13}\text{CN}$  (Fig. C.2), and  $^{13}\text{CH}_3^{13}\text{CH}_2\text{CN}$  (Fig. C.3), respectively. The parameters of these detected lines are listed in Tables 4, 5, and 6, respectively. These tables also contain a few additional lines that we have not counted as formally detected because their wings suffer a bit more from blending with emission from other species (line(s) around 106434 MHz for  $\text{CH}_3^{13}\text{CH}_2^{13}\text{CN}$ , 86938 MHz and 103906 MHz for  $^{13}\text{CH}_3\text{CH}_2^{13}\text{CN}$ , and 85727 MHz and 109313 MHz for  $^{13}\text{CH}_3^{13}\text{CH}_2\text{CN}$ ). They are used in the population diagrams described below.

Figure 1 shows the population diagrams of the three isotopologues that were constructed using most of the lines listed in

Tables 4, 5, and 6. The number of lines shown in the population diagrams does not exactly match the number of detected lines reported above for several reasons. First of all, some detected lines are blends of several transitions of the same molecule with different upper-level energies and thus cannot be plotted in a population diagram. Second, some lines plotted in the population diagrams are somewhat more contaminated by other species than what we require to qualify them as detected. Still we show them in the population diagrams because we can account for this contamination thanks to our full LTE model that contains all species identified so far.

Table 7 lists the results of the rotational temperature fits for the three doubly  $^{13}\text{C}$ -substituted isotopologues, along with the results previously obtained for  $\text{C}_2\text{H}_5\text{CN}$  and the three singly  $^{13}\text{C}$ -substituted isotopologues (Belloche et al. 2016). The uncertainties on the derived rotational temperatures of the doubly  $^{13}\text{C}$ -substituted isotopologues are large because of the small number of transitions and the narrow range spanned by their upper-level energies. Their rotational temperatures are thus poorly constrained but they are consistent within  $1-2\sigma$  with the value of 150 K that we adopted based on  $\text{C}_2\text{H}_5\text{CN}$  and the three singly  $^{13}\text{C}$ -substituted isotopologues (Belloche et al. 2016). Similarly there are too few uncontaminated lines with sufficiently high signal-to-noise ratios to derive the size of the emission accurately on the basis of the integrated intensity maps. Therefore we assume the same source size of  $1.2''$  as for the more abundant isotopologues. The parameters of the best-fit LTE models are listed in Table 8. Those for  $\text{C}_2\text{H}_5\text{CN}$ , the three singly  $^{13}\text{C}$ -substituted isotopologues, and the  $^{15}\text{N}$  isotopologue were already reported in Belloche et al. (2016).

Uncertainties are not reported in Table 8. Each isotopologue has several lines detected with a signal-to-noise ratio close to or above 10 if we consider the peak temperatures, or even 20–40 if we consider the integrated intensities. Therefore, the pure statistical uncertainty on the derived column densities is smaller than 10% if we assume that at least one of the detected lines is free of contamination at its peak or its contamination is well accounted for by our model (otherwise, the column density can only be viewed as an upper limit). Belloche et al. (2016) estimated a calibration uncertainty of 15% for the individual setups of the EMoCA survey. Since the detected lines are distributed among several setups, we do not expect the derived column densities to be biased by the calibration of a particular setup. Therefore the column density uncertainty resulting from the calibration uncertainty should be less than 15%. Taking both sources of uncertainty together (statistics and calibration), the uncertainty on the column density should not be larger than  $\sim 15\%$ . The rotational temperatures were assumed to be equal to those of the more abundant isotopologues (Belloche et al. 2016). Provided this assumption is correct, the uncertainty on the rotational tem-

**Table 4.** Selection of lines of  $\text{CH}_3^{13}\text{CH}_2^{13}\text{CN}$  covered by the EMOCA survey of Sgr B2(N2).

Transition <sup>a</sup>	Frequency (MHz)	Unc. <sup>b</sup> (kHz)	$E_{\text{up}}^c$ (K)	$g_{\text{up}}^d$	$A_{\text{ul}}^e$ ( $10^{-5} \text{ s}^{-1}$ )	$\sigma^f$ (mK)	$\tau_{\text{peak}}^g$	Frequency range <sup>h</sup>		$I_{\text{obs}}^i$ (K km s <sup>-1</sup> )	$I_{\text{mod}}^j$ (K km s <sup>-1</sup> )	$I_{\text{all}}^k$
10 <sub>2,9</sub> – 9 <sub>2,8</sub>	88391.979	1	28	21	5.8	153	0.031	88391.1	88393.5	10.7(6)*	6.7	11.3
10 <sub>4,7</sub> – 9 <sub>4,6</sub>	88700.116	1	41	21	5.1	153	0.034	88699.3	88702.7	11.9(7)*	11.0	12.2
10 <sub>4,6</sub> – 9 <sub>4,5</sub>	88701.248	1	41	21	5.1	–	–	–	–	–	–	–
10 <sub>2,8</sub> – 9 <sub>2,7</sub>	89609.594	1	28	21	6.0	149	0.031	89608.6	89611.1	8.9(5)*	7.2	10.3
11 <sub>0,11</sub> – 10 <sub>0,10</sub>	95857.723	1	28	23	7.7	100	0.038	95856.4	95859.4	12.5(4)*	9.8	10.8
11 <sub>5,7</sub> – 10 <sub>5,6</sub>	97553.481	1	55	23	6.5	100	0.052	97552.5	97555.0	13.6(3)*	12.8	13.4
11 <sub>5,6</sub> – 10 <sub>5,5</sub>	97553.506	1	55	23	6.5	–	–	–	–	–	–	–
11 <sub>1,10</sub> – 10 <sub>1,9</sub>	99642.907	1	30	23	8.6	162	0.039	99641.8	99644.7	7.5(6)*	10.3	11.4
12 <sub>5,8</sub> – 11 <sub>5,7</sub>	106433.758	1	60	25	8.8	123	0.063	106432.3	106435.7	17.2(4)*	13.6	16.0
12 <sub>5,7</sub> – 11 <sub>5,6</sub>	106433.815	1	60	25	8.8	–	–	–	–	–	–	–
12 <sub>3,9</sub> – 11 <sub>3,8</sub>	106684.840	1	43	25	9.3	123	0.040	106683.9	106686.8	12.1(4)*	8.5	9.0
13 <sub>0,13</sub> – 12 <sub>0,12</sub>	112704.985	2	38	27	12.6	242	0.049	112703.9	112706.8	18.4(8)*	14.3	14.9

**Notes.** (a) Quantum numbers of the upper and lower levels. (b) Frequency uncertainty. (c) Upper level energy. (d) Upper level degeneracy. (e) Einstein coefficient for spontaneous emission. (f) Measured rms noise level. (g) Peak opacity of the synthetic line. (h) Frequency range over which the emission was integrated. (i) Integrated intensity of the observed spectrum in brightness temperature scale. The statistical standard deviation is given in parentheses in unit of the last digit. Values marked with a star are used in the population diagrams shown in Figs. 1a and b. (j) Integrated intensity of the synthetic spectrum of  $\text{CH}_3^{13}\text{CH}_2^{13}\text{CN}$ . (k) Integrated intensity of the model that contains the contribution of all identified molecules, including  $\text{CH}_3^{13}\text{CH}_2^{13}\text{CN}$ .

**Table 5.** Selection of lines of  $^{13}\text{CH}_3\text{CH}_2^{13}\text{CN}$  covered by the EMOCA survey of Sgr B2(N2).

Transition <sup>a</sup>	Frequency (MHz)	Unc. <sup>b</sup> (kHz)	$E_{\text{up}}^c$ (K)	$g_{\text{up}}^d$	$A_{\text{ul}}^e$ ( $10^{-5} \text{ s}^{-1}$ )	$\sigma^f$ (mK)	$\tau_{\text{peak}}^g$	Frequency range <sup>h</sup>		$I_{\text{obs}}^i$ (K km s <sup>-1</sup> )	$I_{\text{mod}}^j$ (K km s <sup>-1</sup> )	$I_{\text{all}}^k$
10 <sub>7,3</sub> – 9 <sub>7,2</sub>	86929.429	1	77	21	2.7	142	0.051	86928.2	86931.6	13.8(6)	14.2	14.8
10 <sub>7,4</sub> – 9 <sub>7,3</sub>	86929.429	1	77	21	2.7	–	–	–	–	–	–	–
10 <sub>5,6</sub> – 9 <sub>5,5</sub>	86930.299	1	51	21	4.0	–	–	–	–	–	–	–
10 <sub>5,5</sub> – 9 <sub>5,4</sub>	86930.307	1	51	21	4.0	–	–	–	–	–	–	–
10 <sub>8,2</sub> – 9 <sub>8,1</sub>	86938.144	2	93	21	2.0	142	0.014	86937.0	86939.5	2.9(5)*	3.2	3.5
10 <sub>8,3</sub> – 9 <sub>8,2</sub>	86938.144	2	93	21	2.0	–	–	–	–	–	–	–
11 <sub>0,11</sub> – 10 <sub>0,10</sub>	94120.285	2	27	23	7.2	104	0.036	94119.0	94121.9	9.2(4)*	6.8	7.2
11 <sub>6,6</sub> – 10 <sub>6,5</sub>	95623.286	1	67	23	5.0	100	0.041	95622.0	95627.4	18.7(5)	18.8	21.8
11 <sub>6,5</sub> – 10 <sub>6,4</sub>	95623.286	1	67	23	5.0	–	–	–	–	–	–	–
11 <sub>7,4</sub> – 10 <sub>7,3</sub>	95625.196	1	82	23	4.2	–	–	–	–	–	–	–
11 <sub>7,5</sub> – 10 <sub>7,4</sub>	95625.196	1	82	23	4.2	–	–	–	–	–	–	–
11 <sub>2,9</sub> – 10 <sub>2,8</sub>	96704.440	2	32	23	7.6	155	0.036	96702.9	96706.4	11.6(6)*	9.4	11.5
12 <sub>2,11</sub> – 11 <sub>2,10</sub>	103905.981	2	37	25	9.5	114	0.041	103905.0	103907.9	10.9(4)*	8.4	8.7
12 <sub>7,5</sub> – 11 <sub>7,4</sub>	104321.766	1	87	25	6.1	114	0.088	104320.6	104324.1	21.0(4)	18.9	26.3
12 <sub>7,6</sub> – 11 <sub>7,5</sub>	104321.766	1	87	25	6.1	–	–	–	–	–	–	–
12 <sub>6,7</sub> – 11 <sub>6,6</sub>	104322.135	1	72	25	6.9	–	–	–	–	–	–	–
12 <sub>6,6</sub> – 11 <sub>6,5</sub>	104322.135	1	72	25	6.9	–	–	–	–	–	–	–
12 <sub>2,10</sub> – 11 <sub>2,9</sub>	105682.862	2	37	25	10.0	123	0.041	105681.6	105685.0	10.7(5)*	9.1	11.2
13 <sub>2,12</sub> – 12 <sub>2,11</sub>	112499.968	2	42	27	12.2	166	0.047	112498.4	112501.8	19.7(6)*	13.5	16.4

**Notes.** (a) Quantum numbers of the upper and lower levels. (b) Frequency uncertainty. (c) Upper level energy. (d) Upper level degeneracy. (e) Einstein coefficient for spontaneous emission. (f) Measured rms noise level. (g) Peak opacity of the synthetic line. (h) Frequency range over which the emission was integrated. (i) Integrated intensity of the observed spectrum in brightness temperature scale. The statistical standard deviation is given in parentheses in unit of the last digit. Values marked with a star are used in the population diagrams shown in Figs. 1c and d. (j) Integrated intensity of the synthetic spectrum of  $^{13}\text{CH}_3\text{CH}_2^{13}\text{CN}$ . (k) Integrated intensity of the model that contains the contribution of all identified molecules, including  $^{13}\text{CH}_3\text{CH}_2^{13}\text{CN}$ .

peratures does not have a significant impact on the relative abundance ratios which are discussed in Sect. 4.2. The same is true for the source size and linewidth.

## 4. Discussion

### 4.1. Laboratory spectroscopy

It can be seen in Table 1 that substitution of two of the three  $^{12}\text{C}$  atoms in the main isotopologue of ethyl cyanide by  $^{13}\text{C}$  causes only slight decreases in the rotational parameters  $A$ ,  $B$  and  $C$ . It is therefore not surprising that the magnitudes of the centrifugal distortion parameters also change only slightly, in particular

**Table 6.** Selection of lines of  $^{13}\text{CH}_3^{13}\text{CH}_2\text{CN}$  covered by the EMOCA survey of Sgr B2(N2).

Transition <sup>a</sup>	Frequency (MHz)	Unc. <sup>b</sup> (kHz)	$E_{\text{up}}^c$ (K)	$g_{\text{up}}^d$	$A_{\text{ul}}^e$ ( $10^{-5} \text{ s}^{-1}$ )	$\sigma^f$ (mK)	$\tau_{\text{peak}}^g$	Frequency range <sup>h</sup> (MHz)		$I_{\text{obs}}^i$ (K km s <sup>-1</sup> )	$I_{\text{mod}}^j$ (K km s <sup>-1</sup> )	$I_{\text{all}}^k$
10 <sub>0,10</sub> – 9 <sub>0,9</sub>	85729.089	4	23	21	5.5	158	0.030	85727.9	85730.9	12.2(7)*	7.0	8.9
10 <sub>5,6</sub> – 9 <sub>5,5</sub>	86999.357	4	50	21	4.3	142	0.038	86998.1	87001.0	9.4(6)*	9.2	9.3
10 <sub>5,5</sub> – 9 <sub>5,4</sub>	86999.366	4	50	21	4.3	–	–	–	–	–	–	–
10 <sub>4,7</sub> – 9 <sub>4,6</sub>	87022.337	4	40	21	4.8	142	0.033	87021.5	87024.9	14.7(6)*	10.8	11.6
10 <sub>4,6</sub> – 9 <sub>4,5</sub>	87023.409	4	40	21	4.8	–	–	–	–	–	–	–
10 <sub>1,9</sub> – 9 <sub>1,8</sub>	88957.082	4	25	21	6.0	153	0.032	88955.7	88958.6	7.4(6)*	7.1	8.9
11 <sub>1,11</sub> – 10 <sub>1,10</sub>	92623.369	4	28	23	6.9	117	0.035	92622.3	92625.2	8.6(5)*	6.5	6.6
11 <sub>3,8</sub> – 10 <sub>3,7</sub>	95882.623	1	37	23	6.6	100	0.032	95881.8	95884.3	11.9(3)	7.9	10.1
11 <sub>2,9</sub> – 10 <sub>2,8</sub>	96879.471	4	32	23	7.7	155	0.034	96878.3	96881.2	8.0(6)*	9.1	9.3
12 <sub>0,12</sub> – 11 <sub>0,11</sub>	102350.118	4	32	25	9.4	141	0.042	102348.8	102352.2	13.7(5)*	11.8	11.8
12 <sub>2,11</sub> – 11 <sub>2,10</sub>	103952.061	4	37	25	9.6	114	0.040	103950.9	103953.8	12.0(4)*	8.4	10.0
13 <sub>1,13</sub> – 12 <sub>1,12</sub>	109312.610	4	38	27	11.4	123	0.047	109311.1	109314.5	18.7(4)*	14.2	18.5

**Notes.** (a) Quantum numbers of the upper and lower levels. (b) Frequency uncertainty. (c) Upper level energy. (d) Upper level degeneracy. (e) Einstein coefficient for spontaneous emission. (f) Measured rms noise level. (g) Peak opacity of the synthetic line. (h) Frequency range over which the emission was integrated. (i) Integrated intensity of the observed spectrum in brightness temperature scale. The statistical standard deviation is given in parentheses in unit of the last digit. Values marked with a star are used in the population diagrams shown in Figs. 1e and f. (j) Integrated intensity of the synthetic spectrum of  $^{13}\text{CH}_3^{13}\text{CH}_2\text{CN}$ . (k) Integrated intensity of the model that contains the contribution of all identified molecules, including  $^{13}\text{CH}_3^{13}\text{CH}_2\text{CN}$ .

**Table 7.** Rotational temperatures derived from population diagrams of ethyl cyanide and its isotopologues toward Sgr B2(N2).

Molecule	States <sup>a</sup>	$T_{\text{fit}}^b$ (K)
$\text{C}_2\text{H}_5\text{CN}^c$	$v = 0$	137.3 (1.6)
$^{13}\text{CH}_3\text{CH}_2\text{CN}^c$	$v = 0$	138.3 (7.5)
$\text{CH}_3^{13}\text{CH}_2\text{CN}^c$	$v = 0$	112 (11)
$\text{CH}_3\text{CH}_2^{13}\text{CN}^c$	$v = 0$	150 (40)
$^{13}\text{CH}_3^{13}\text{CH}_2\text{CN}$	$v = 0$	70 (40)
$^{13}\text{CH}_3\text{CH}_2^{13}\text{CN}$	$v = 0$	96 (66)
$\text{CH}_3^{13}\text{CH}_2^{13}\text{CN}$	$v = 0$	122 (77)

**Notes.** (a) Vibrational states that were taken into account to fit the population diagram. (b) The standard deviation of the fit is given in parentheses. As explained in Sect. 3 of Belloche et al. (2016), these uncertainties should be viewed with caution. They may be underestimated. (c) For these species, the analysis was performed in Belloche et al. (2016).

those of lower order. It may surprise at first that some of the distortion parameters of the doubly  $^{13}\text{C}$ -substituted isotopologues are actually larger than those of the main species. One should, however, keep in mind that one finds empirically that the distortion parameters scale approximately with appropriate powers of  $A - (B + C)/2$ ,  $B + C$  and  $B - C$ . The line lists of the three doubly  $^{13}\text{C}$ -substituted ethyl cyanide isotopologues differ somewhat, which easily explains changes in the uncertainties among these isotopologues.

#### 4.2. Astronomical observations

The column densities reported in Table 8 imply a  $^{12}\text{C}^{12}\text{C}/^{12}\text{C}^{13}\text{C}$  ratio of  $\sim 32$  and a  $^{12}\text{C}^{13}\text{C}/^{13}\text{C}^{13}\text{C}$  ratio of  $\sim 25$  for ethyl cyanide in Sgr B2(N2). The  $^{12}\text{C}^{13}\text{C}/^{13}\text{C}^{13}\text{C}$  ratio derived for ethyl cyanide is very similar to the  $^{12}\text{C}^{13}\text{C}/^{13}\text{C}^{13}\text{C}$  ratio tentatively obtained for  $\text{HC}_3\text{N}$  in the same source ( $\sim 24$ , see Belloche et al. 2016) and to the  $^{12}\text{C}/^{13}\text{C}$  ratio derived for methanol and ethanol ( $\sim 25$ , see Müller et al. 2016). However, the difference on the or-

**Table 8.** Parameters of our best-fit LTE model of ethyl cyanide and its isotopologues toward Sgr B2(N2).

Molecule	$N_{\text{det}}^a$	$N^b$ (cm <sup>-2</sup> )	$F_{\text{vib}}^c$	$\frac{N_{\text{ref}}^d}{N}$
$\text{C}_2\text{H}_5\text{CN}^e$	154	6.2 (18)	1.38	1
$^{13}\text{CH}_3\text{CH}_2\text{CN}^e$	54	1.9 (17)	1.38	32
$\text{CH}_3^{13}\text{CH}_2\text{CN}^e$	38	1.9 (17)	1.38	32
$\text{CH}_3\text{CH}_2^{13}\text{CN}^e$	37	1.9 (17)	1.38	32
$^{13}\text{CH}_3^{13}\text{CH}_2\text{CN}$	8	7.6 (15)	1.38	818
$^{13}\text{CH}_3\text{CH}_2^{13}\text{CN}$	8	7.6 (15)	1.38	818
$\text{CH}_3^{13}\text{CH}_2^{13}\text{CN}$	7	7.6 (15)	1.38	818
$\text{C}_2\text{H}_5\text{C}^{15}\text{N}^e$	9	1.2 (16)	1.38	500

**Notes.** For all species, the model assumes a source size of  $1.20''$ , a rotational temperature of 150 K, a linewidth of  $5.0 \text{ km s}^{-1}$ , and a velocity offset of  $-0.8 \text{ km s}^{-1}$  with respect to the assumed systemic velocity of Sgr B2(N2),  $V_{\text{lsr}} = 74 \text{ km s}^{-1}$ . (a) Number of detected lines (conservative estimate, see Sect. 3 of Belloche et al. 2016). One line of a given species may mean a group of transitions of that species that are blended together. (b) Total column density of the molecule.  $X (Y)$  means  $X \times 10^Y$ . (c) Correction factor that was applied to the column density to account for the contribution of vibrationally excited states. (d) Column density ratio, with  $N_{\text{ref}}$  the column density of  $\text{C}_2\text{H}_5\text{CN}$ . (e) For these species, the analysis was performed in Belloche et al. (2016).

der of 25% between the  $^{12}\text{C}^{12}\text{C}/^{12}\text{C}^{13}\text{C}$  and  $^{12}\text{C}^{13}\text{C}/^{13}\text{C}^{13}\text{C}$  ratios of ethyl cyanide is a priori surprising. Given that the main isotopologue and the singly  $^{13}\text{C}$ -substituted ones have a much larger number of detected lines than the doubly  $^{13}\text{C}$ -substituted ones, the uncertainty on the column densities of the former should be much smaller than the upper limit of 15% estimated for the latter in Sect. 3.2. Therefore the difference between the two ratios seems to be significant. The two ratios would be reconciled with a value of 28.6 if the column densities of the singly  $^{13}\text{C}$ -substituted isotopologues were higher by a factor 1.12, which would correspond to a vertical increment of 0.11 in their population diagrams (see Figs. 7b, 8b, and 9b of Belloche et al. 2016). Such an increment is not completely excluded, but it seems to be marginally consistent with the observed spectra, given the large

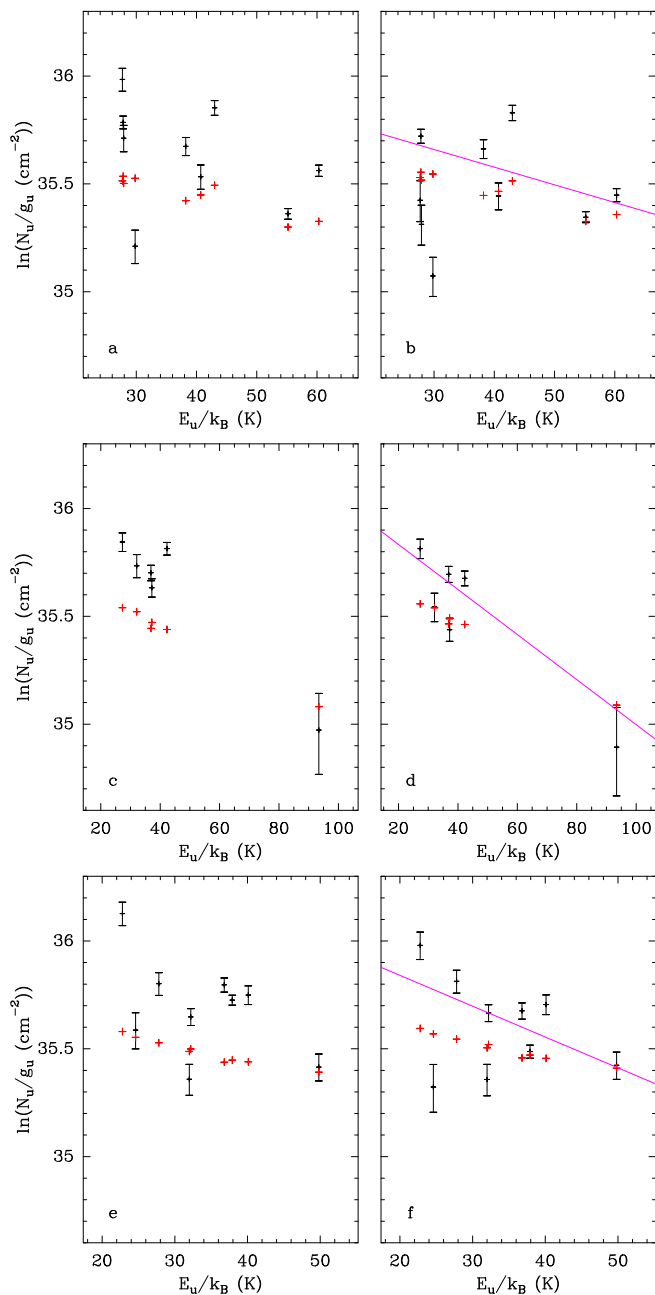


**Fig. 1.** **a, b** Population diagram of  $\text{CH}_3^{13}\text{CH}_2^{13}\text{CN}$ ,  $v = 0$  toward Sgr B2(N2). Only the lines that are clearly detected and do not suffer too much from contamination from other species are displayed. The observed datapoints are shown in black while the synthetic populations are shown in red. No correction is applied in panel **a**. In panel **b**, the optical depth correction has been applied to both the observed and synthetic populations and the contamination from all other species included in the full model has been removed from the observed datapoints. The purple line is a linear fit to the observed populations (in linear-logarithmic space). The derived rotation temperature is given in Table 7. **c, d** Same as **a, b** for  $^{13}\text{CH}_3\text{CH}_2^{13}\text{CN}$ ,  $v = 0$ . **e, f** Same as **a, b** for  $^{13}\text{CH}_3^{13}\text{CH}_2\text{CN}$ ,  $v = 0$ .

number of detected transitions and the fact that a few of them are already somewhat overestimated by the current model. The fact that the  $^{12}\text{C}^{12}\text{C}/^{12}\text{C}^{13}\text{C}$  ratio is higher than the  $^{12}\text{C}^{13}\text{C}/^{13}\text{C}^{13}\text{C}$  ratio cannot be due to an optical depth effect either because saturation of ethyl cyanide transitions, if not properly taken into account, would tend to decrease the apparent  $^{12}\text{C}^{12}\text{C}/^{12}\text{C}^{13}\text{C}$  ratio compared to the  $^{12}\text{C}^{13}\text{C}/^{13}\text{C}^{13}\text{C}$  ratio. Our analysis takes into

account the line optical depth and we excluded the lines that are too opaque ( $\tau < 2.5$ , see Fig. 6 of Belloche et al. 2016), so we believe that the  $^{12}\text{C}^{12}\text{C}/^{12}\text{C}^{13}\text{C}$  ratio is not affected by an opacity bias. Another possibility is that the column density of the doubly  $^{13}\text{C}$ -substituted isotopologues is overestimated by a factor  $\sim 1.3$ . Given that the EMOCA spectrum is close to the confusion limit, this cannot be excluded as long as there are still unidentified lines in the survey.

Finally, we cannot exclude that our assumption of a uniform source structure and the use of the same source size for all isotopologues introduce systematic biases in the derived column densities. Figure 10 of Belloche et al. (2016) shows that the source size actually depends on the upper-level energy of the detected transitions of ethyl cyanide. A more elaborated model taking into account the temperature, density, and possibly abundance gradients in Sgr B2(N2) would be necessary to verify whether the difference between the  $^{12}\text{C}^{12}\text{C}/^{12}\text{C}^{13}\text{C}$  and  $^{12}\text{C}^{13}\text{C}/^{13}\text{C}^{13}\text{C}$  ratios obtained through our simple analysis is significant or not.

## 5. Conclusions

We have unambiguously detected the three isotopomers of ethyl cyanide with two  $^{13}\text{C}$  atoms in the Sgr B2(N2) hot core. Ethyl cyanide is the second molecule after methyl cyanide (Belloche et al. 2016) for which isotopologues containing two  $^{13}\text{C}$  atoms have been securely detected in the interstellar medium. The  $^{12}\text{C}/^{13}\text{C}$  column density ratio between ethyl cyanide isotopomers with one  $^{13}\text{C}$  atom and those with two  $^{13}\text{C}$  atoms is  $\sim 25$ , in good agreement with ratios reported for several other molecules in this source. The  $^{12}\text{C}/^{13}\text{C}$  ratio between the main isotopologue and the ones with one  $^{13}\text{C}$  atom is higher ( $\sim 32$ ), but it is unclear at this stage whether this is a significant difference or a bias due to our simple assumptions about the physical structure of the source. The signal-to-noise ratios of the detected lines and the derived (rotational) temperature of 150 K suggest that vibrational satellites of the isotopologues with two  $^{13}\text{C}$  atoms may be just too weak to be identified unambiguously in our current dataset. We expect, however, to be able to identify vibrational satellites of the isotopologues with one  $^{13}\text{C}$  atom up to the three states with  $v_{13} + v_{21} = 2$  at  $\sim 600$  K, possibly even those of  $v_{12} = 1$  at  $\sim 770$  K. Vibrational satellites of the main species should be observable up to at least  $v_{19} = 1$  at  $\sim 1130$  K.

*Acknowledgements.* The present investigations were supported by the CNES and the CNRS program “Physique et Chimie du Milieu Interstellaire” (PCMI). This work was also done under ANR-13-BS05-0008-02 IMOLABS. Support by the Deutsche Forschungsgemeinschaft (DFG) in the framework of the collaborative research grant SFB 956, project B3 is also acknowledged. This paper makes use of the following ALMA data: ADS/JAO.ALMA#2011.0.00017.S, ADS/JAO.ALMA#2012.1.00012.S. ALMA is a partnership of ESO (representing its member states), NSF (USA) and NINS (Japan), together with NRC (Canada), NSC and ASIAA (Taiwan), and KASI (Republic of Korea), in cooperation with the Republic of Chile. The Joint ALMA Observatory is operated by ESO, AUI/NRAO and NAOJ. The interferometric data are available in the ALMA archive at <https://almascience.eso.org/aq/>.

## References

- Alekseev, E. A., Motiyenko, R. A., Margulès, L. 2012, *Radio Phys. Radio Astron.*, 3, 75
- Belloche, A., Menten, K. M., Comito, C., et al. 2008, *A&A*, 482, 179
- Belloche, A., Garrod, R. T., Müller, H. S. P., et al. 2009, *A&A*, 499, 215
- Belloche, A., Müller, H. S. P., Menten, K. M., Schilke, P., & Comito, C. 2013, *A&A*, 559, A47
- Belloche, A., Garrod, R. T., Müller, H. S. P., & Menten, K. M. 2014, *Science*, 345, 1584

- Belloche, A., Müller, H. S. P., Garrod, R. T., & Menten, K. M. 2016, *A&A*, 587, A91
- Bossa, J.-B., Ordu, M. H., Müller, H. S. P., Lewen, F., & Schlemmer, S. 2014, *A&A*, 570, A12
- Bouchez, A., Walters, A., Müller, H. S. P., et al. 2012, *J. Quant. Spectrosc. Radiat. Transfer*, 113, 1148
- Brauer, C. S., Pearson, J. C., Drouin, B. J., & Yu, S. 2009, *ApJS*, 184, 133
- Cazaux, S., Tielens, A. G. G. M., Ceccarelli, C., et al. 2003, *ApJ*, 593, L51
- Daly, A. M., Bermúdez, C., López, A., et al. 2013, *ApJ*, 768, 81
- Demyk, K., Mäder, H.; Tercero, B.; et al. 2007, *A&A*, 466, 255
- Gibb, E., Nummelin, A., Irvine, W. M., Whittet, D. C. B., & Bergman, P. 2000, *ApJ*, 545, 309
- Heise, H. M., Winther, F., & Lutz, H. 1981, *J. Mol. Spectrosc.*, 90, 531
- Johnson, D. R., Lovas, F. J., Gottlieb, C. A., et al. 1977, *ApJ*, 218, 370
- Kisiel, Z. 2001, *Spectroscopy from Space* (Dordrecht: Kluwer Academic Publishers), see also PROSPE - Programs for ROTational SPEctroscopy, <http://info.ifpan.edu.pl/~kisiel/prospe.htm>
- Kraśnicki, A., & Kisiel, Z. 2011, *J. Mol. Spectrosc.*, 270, 83
- Margulès, L., Motiyenko, R., Demyk, K., et al. 2009, *A&A*, 493, 565
- Mehring, D. M., Pearson, J. C., Keene, J., & Phillips, T. G. 2004, *ApJ*, 608, 306
- Milam, S. N., Savage, C., Brewster, M. A., Ziurys, L. M., & Wyckoff, S. 2005, *ApJ*, 634, 1126
- Møllendal, H., Margulès, L., Belloche, A., et al. 2012, *A&A*, 538, A51
- Motiyenko, R. A., Margulès, L., & Guillemin, J.-C. 2013, *A&A*, 559, A44
- Motoki, Y., Tsunoda, Y., Ozeki, H., & Kobayashi, K. 2013, *ApJSS*, 209, 23
- Müller, H. S. P., Thorwirth, S., Roth, D. A., & Winnewisser, G. 2001, *A&A*, 370, L49
- Müller, H. S. P., Schlöder, F., Stutzki, J., & Winnewisser, G. 2005, *J. Mol. Struct.*, 742, 215
- Müller, H. S. P., Belloche, A., Menten, K. M., et al. 2008, *J. Mol. Spectrosc.*, 251, 319
- Müller, H. S. P., Coutens, A., Walters, A., et al. 2011, *J. Mol. Spectrosc.*, 267, 100
- Müller, H. S. P., Belloche, A., Xu, L.-H., et al. 2016, *A&A*, 587, A92
- Neill, J. L., Bergin, E. A., Lis, D. C., et al. 2014, *ApJ*, 789, 8
- Nummelin, A., Bergman, P., Hjalmarson, Å., et al. 1998, *ApJS*, 117, 427
- Nummelin, A., Bergman, P., Hjalmarson, Å., et al. 2000, *ApJS*, 128, 213
- Ordu, M. H., Müller, H. S. P., Walters, A., et al. 2012, *A&A*, 541, A121
- Pickett, H. M. 1991, *J. Mol. Spectrosc.*, 148, 371
- Pickett, H. M., Poynter, R. L., Cohen, E. A., et al. 1998, *J. Quant. Spectrosc. Radiat. Transfer*, 60, 883
- Qin, S.-L., Schilke, P., Rolfes, R., et al. 2011, *A&A*, 530, LL9
- Richard, C., Margulès, L., Motiyenko, R. A., & Guillemin, J.-C. 2012, *A&A*, 543, A135
- Solomon, P. M., Jefferts, K. B., Penzias, A. A., & Wilson, R. W. 1971, *ApJ*, 168, L107
- Taquet, V., López-Sepulcre, A., Ceccarelli, C., et al. 2015, *ApJ*, 804, 81



## Appendix A: Nuclear magnetic resonance data

The NMR type is given first with solvent and the resonance frequency are given in parentheses, the shift  $\delta$  in ppm with appearance pattern (d, t, q stands for doublet, triplet, quartet), the origin of the pattern is given in case of the  $^1\text{H}$  NMR, spin-spin coupling parameters  $^{n+1}J_{\text{AB}}$  in parentheses, the originating molecule group is given at the end; A and B are the respective nuclei, and  $n$  is the number of atoms between A and B.

### Propanenitrile-1,2- $^{13}\text{C}_2$

$^1\text{H}$  NMR ( $\text{CDCl}_3$ , 400 MHz):

$\delta$  1.29 (ddt, 3H,  $^2J_{\text{CH}} = 4.6$  Hz,  $^3J_{\text{CH}} = 6.6$  Hz,  $^3J_{\text{HH}} = 7.7$  Hz,  $\text{CH}_3$ )  
 $\delta$  2.35 (ddq, 2H,  $^1J_{\text{CH}} = 134.9$  Hz,  $^2J_{\text{CH}} = 9.9$  Hz,  $^3J_{\text{HH}} = 7.7$  Hz,  $\text{CH}_2$ )

$^{13}\text{C}$  NMR ( $\text{CDCl}_3$ , 100 MHz):

$\delta$  10.5 (qdd,  $^1J_{\text{CH}} = 126.1$  Hz,  $^1J_{\text{CC}} = 33.0$  Hz,  $^2J_{\text{CC}} = 4.2$  Hz,  $\text{CH}_3$ )  
 $\delta$  11.1 (td,  $^1J_{\text{CH}} = 135.0$  Hz,  $^1J_{\text{CC}} = 56.0$  Hz,  $\text{CH}_2$ )  
 $\delta$  120.8 (d,  $^1J_{\text{CC}} = 56.0$  Hz, CN)

### Propanenitrile-1,3- $^{13}\text{C}_2$

$^1\text{H}$  NMR ( $\text{CDCl}_3$ , 400 MHz):

$\delta$  1.29 (ddt, 3H,  $^1J_{\text{CH}} = 126.1$  Hz,  $^3J_{\text{CH}} = 6.6$  Hz,  $^3J_{\text{HH}} = 7.7$  Hz,  $\text{CH}_3$ )  
 $\delta$  2.35 (ddq, 2H,  $^2J_{\text{CH}} = 5.0$  Hz,  $^2J_{\text{CH}} = 9.7$  Hz,  $^3J_{\text{HH}} = 7.7$  Hz,  $\text{CH}_2$ )

$^{13}\text{C}$  NMR ( $\text{CDCl}_3$ , 100 MHz):

$\delta$  10.5 (qd,  $^1J_{\text{CH}} = 126.1$  Hz,  $^2J_{\text{CC}} = 4.2$  Hz,  $\text{CH}_3$ )  
 $\delta$  11.1 (tdd,  $^1J_{\text{CH}} = 135.0$  Hz,  $^1J_{\text{CC}} = 56.0$  Hz,  $^1J_{\text{CC}} = 33.0$  Hz,  $\text{CH}_2$ )  
 $\delta$  120.8 (d,  $^2J_{\text{CC}} = 4.2$  Hz, CN)

### Propanenitrile-2,3- $^{13}\text{C}_2$

$^1\text{H}$  NMR ( $\text{CDCl}_3$ , 400 MHz):

$\delta$  1.30 (ddt, 3H,  $^1J_{\text{CH}} = 126.1$  Hz,  $^2J_{\text{CH}} = 4.6$  Hz,  $^3J_{\text{HH}} = 7.7$  Hz,  $\text{CH}_3$ )  
 $\delta$  2.35 (dq, 2H,  $^1J_{\text{CH}} = 135.0$  Hz,  $^3J_{\text{HH}} = 7.7$  Hz,  $^2J_{\text{CH}} = 5.0$  Hz,  $\text{CH}_2$ )

$^{13}\text{C}$  NMR ( $\text{CDCl}_3$ , 100 MHz):

$\delta$  10.5 (qd,  $^1J_{\text{CH}} = 126.1$  Hz,  $^1J_{\text{CC}} = 33.0$  Hz,  $\text{CH}_3$ )  
 $\delta$  11.1 (td,  $^1J_{\text{CH}} = 135.0$  Hz,  $^1J_{\text{CC}} = 33.0$  Hz,  $\text{CH}_2$ )  
 $\delta$  120.8 (dd,  $^1J_{\text{CC}} = 56.0$  Hz,  $^2J_{\text{CC}} = 4.2$  Hz, CN)

## Appendix B: Experimental data

The experimental transition frequencies of the doubly  $^{13}\text{C}$ -substituted isotopomers of ethyl cyanide are available as supplementary material. The files S1.txt, S2.txt and S3.txt refer to the 1,2-, 1,3- and 2,3-substituted isotopomers, respectively. Only the first 10 and the last 11 lines of the 1,2-species appear in Table B.1; for complete versions of all isotopomers see the electronic edition<sup>3</sup>. The files give the rotational quantum numbers  $J$ ,  $K_a$ , and  $K_c$  for the upper state followed by those for the lower state. The observed transition frequency is given in megahertz units with its uncertainty and the residual between observed frequency and that calculated from the final set of spectroscopic parameters. Blended transitions are treated by fitting the intensity-averaged frequency, and this weight is also given in the tables. In most cases, the blending is caused by unresolved asymmetry splitting, i.e., the blended transitions agree in terms of their quantum numbers except for  $K_c$  (prolate paired transitions) or  $K_a$  (oblate paired transitions), and both transitions are equal in intensity. Accidental blending of transitions occurred occasionally.

## Appendix C: Additional figures

Figures C.1, C.2, and C.3 show the astronomical detections of the three doubly  $^{13}\text{C}$ -substituted isotopologues of ethyl cyanide toward Sgr B2(N2).

<sup>3</sup> <http://cdsarc.ustrasbg.fr/cgi-bin/VizieR?-source=J/A+A/Vol/Num>

**Table B.1.** Experimental data for the 1,2-isotopomer of ethyl cyanide.

Nr.:	$J'$	$K'_a$	$K'_c$	$J''$	$K''_a$	$K''_c$	Frequency	Unc.	O–C	Weight
1:	17	1	17	16	0	16	150042.190	0.030	0.01469	
2:	33	2	31	33	1	32	150331.396	0.030	0.02378	
3:	42	5	37	41	6	36	150403.376	0.030	0.04998	
4:	18	0	18	17	1	17	150425.187	0.030	–0.00721	
5:	17	8	9	16	8	8	150780.154	0.030	–0.00667	0.5000
6:	17	8	10	16	8	9	150780.154	0.030	–0.00667	0.5000
7:	17	9	8	16	9	7	150784.377	0.030	–0.00577	0.5000
8:	17	9	9	16	9	8	150784.377	0.030	–0.00577	0.5000
9:	17	7	10	16	7	9	150789.125	0.030	–0.00886	0.5000
10:	17	7	11	16	7	10	150789.125	0.030	–0.00886	0.5000
6810:	28	17	11	27	16	12	985858.551	0.030	0.02324	0.5000
6811:	28	17	12	27	16	11	985858.551	0.030	0.02324	0.5000
6812:	64	10	54	63	9	55	986054.883	0.030	–0.00124	
6813:	33	16	17	32	15	18	986740.931	0.030	0.00118	0.5000
6814:	33	16	18	32	15	17	986740.931	0.030	0.00118	0.5000
6815:	48	13	35	47	12	36	987077.762	0.030	–0.01559	0.5000
6816:	48	13	36	47	12	35	987077.762	0.030	–0.01559	0.5000
6817:	38	15	23	37	14	24	987305.187	0.030	–0.07257	0.5000
6818:	38	15	24	37	14	23	987305.187	0.030	–0.07257	0.5000
6819:	43	14	29	42	13	30	987468.359	0.030	0.01296	0.5000
6820:	43	14	30	42	13	29	987468.359	0.030	0.01296	0.5000

**Notes.** The table contains the line number, rotational quantum numbers of the assigned transition, observed transition frequency (MHz), experimental uncertainty (MHz), residual O–C between observed frequency and that calculated from the final set of spectroscopic parameters, and weight for blended lines. This table as well as those of other conformers are available in their entirety in the electronic edition in the online journal: <http://cdsarc.ustrasbg.fr/cgi-bin/VizieR?-source=J/A+A/Vol/Num>. A portion is shown here for guidance regarding its form and content.

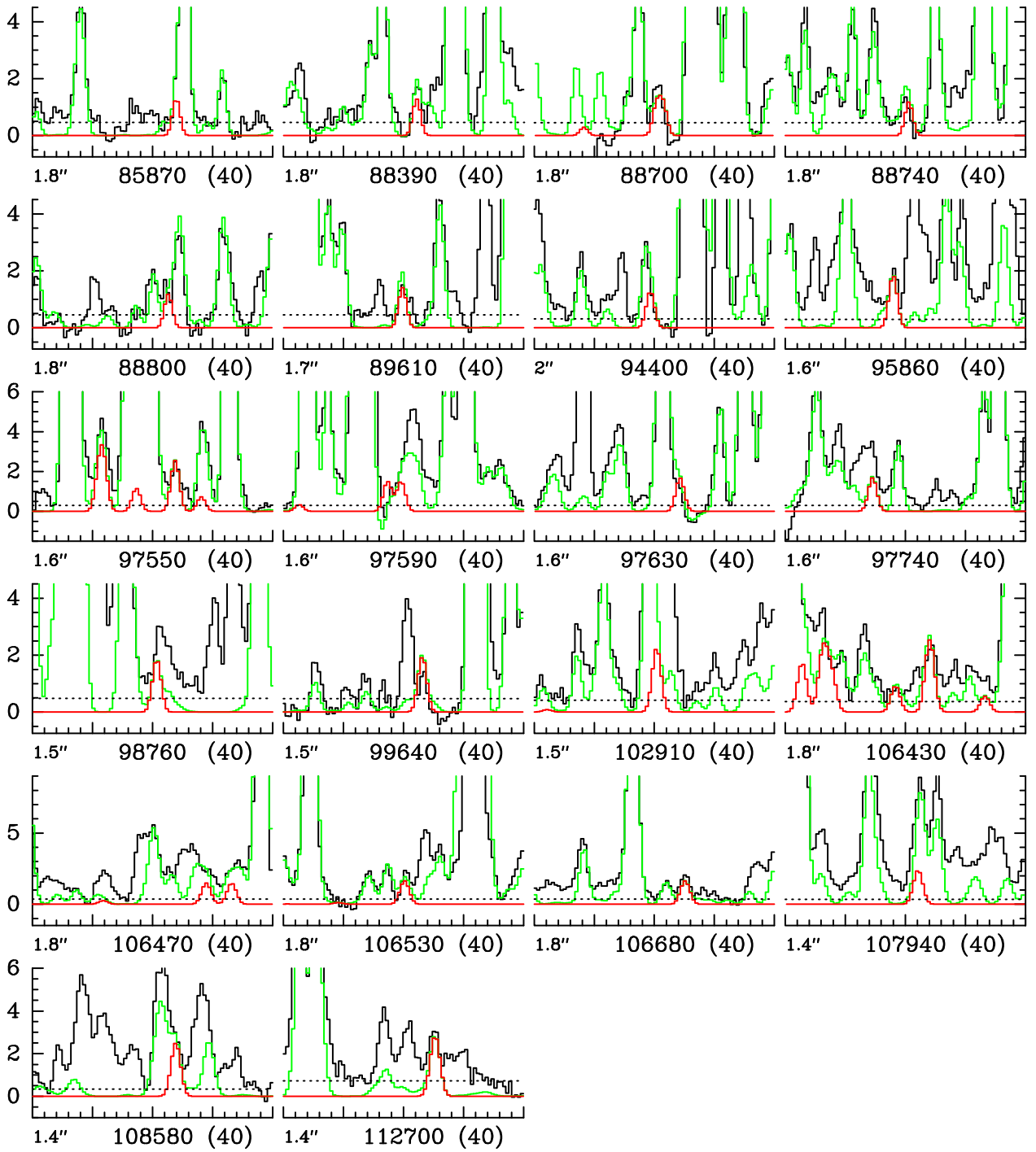


**Fig. C.1.** Transitions of  $\text{CH}_3^{13}\text{CH}_2^{13}\text{CN}$ ,  $v = 0$  covered by our ALMA survey. The best-fit LTE synthetic spectrum of  $\text{CH}_3^{13}\text{CH}_2^{13}\text{CN}$  is displayed in red and overlaid on the observed spectrum of Sgr B2(N2) shown in black. The green synthetic spectrum contains the contributions of all molecules identified in our survey so far, including the one shown in red. The central frequency and width are indicated in MHz below each panel. The angular resolution (HPBW) is also indicated. The y-axis is labeled in brightness temperature units (K). The dotted line indicates the  $3\sigma$  noise level.

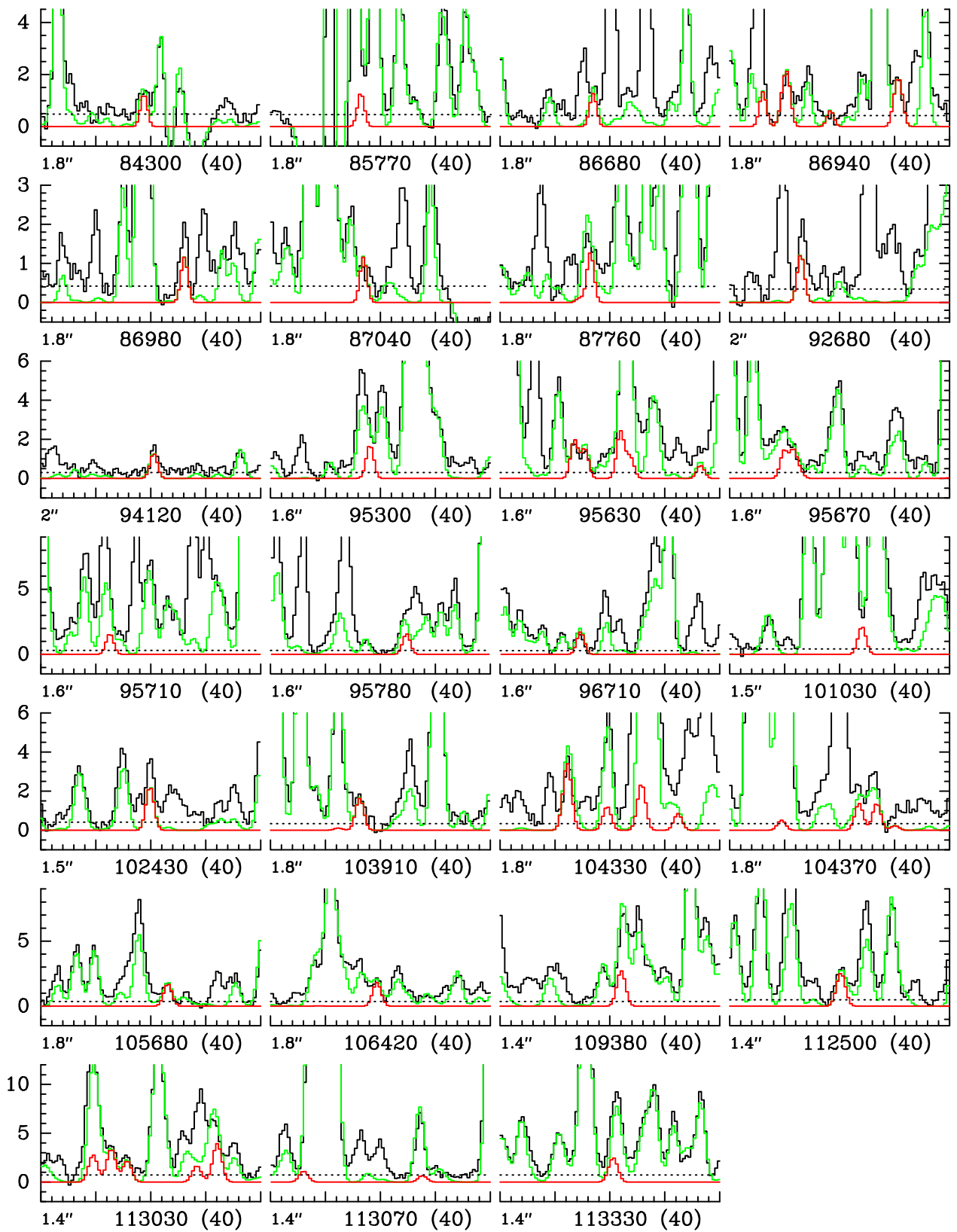


Fig. C.2. Same as Fig. C.1 for  $^{13}\text{CH}_3\text{CH}_2^{13}\text{CN}$ ,  $v = 0$ .

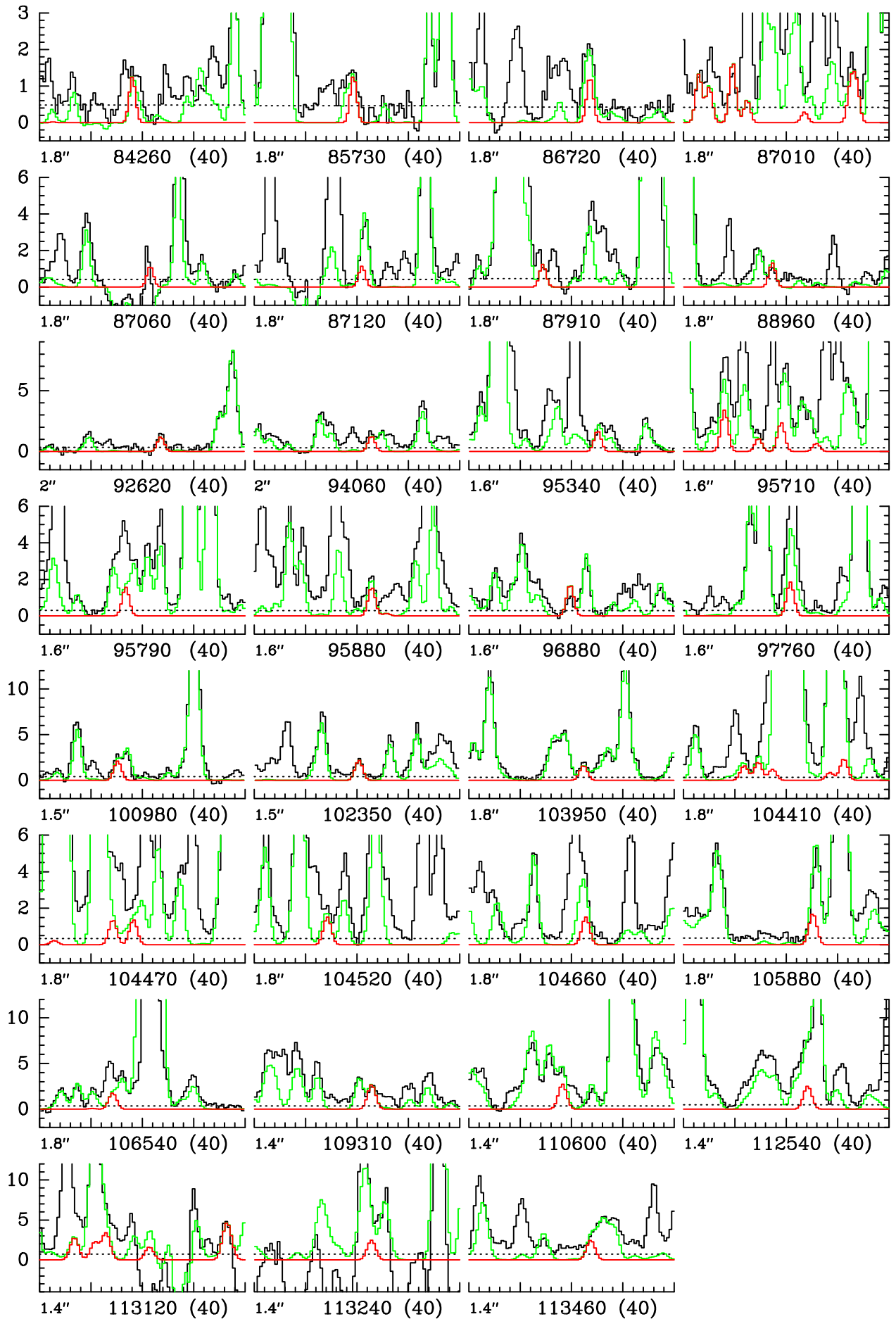


Fig. C.3. Same as Fig. C.1 for  $^{13}\text{CH}_3^{13}\text{CH}_2\text{CN}$ ,  $v=0$ .